The indirect sensing of alkali metal counterions using P3HT-based organic electrochemical transistors working in the accumulation mode

Tatiana Gregorio, Dominique Mombrú, Mariano Romero, Alvaro W Mombrú

ACS Applied Electronic Materials 2025, 7, 15, 6846-6858.

Publisher: American Chemical Society

The indirect sensing of alkali metal counterions using P3HT-based organic electrochemical transistors working in the accumulation mode

Tatiana Gregorio, Dominique Mombrú*, Mariano Romero*, Alvaro W. Mombrú*.

Centro NanoMat & Área Física, Departamento de Experimentación y Teoría de la Estructura de la Materia y sus Aplicaciones (DETEMA), Facultad de Química, Universidad de la República, Montevideo C.P. 11800, Uruguay.

* Corresponding authors:

Dr. Dominique Mombrú (dmombru@fq.edu.uy)

Dr. Mariano Romero (mromero@fq.edu.uy)

Dr. Alvaro W. Mombrú (amombru@fq.edu.uy)

Abstract

Here, we report the alkali metal counterion effect and their corresponding indirect sensing using poly(3-hexylthiophene)-based OECT devices working in the accumulation mode with bis(trifluoromethanesulfonyl)imidate salts aqueous solution as electrolytes. Our *in-operando* microRaman imaging studies confirmed that the charge transport and transfer processes are associated with the accumulation mode configuration, while our *in-operando* X-ray scattering studies indicate that the injection of dopants not only reached the swollen amorphous but also the crystalline regions of poly(3-hexylthiophene) (P3HT). Interestingly, we have observed characteristic features depending on the alkali metal counterion in both output and transfer characteristics for these OECT devices. The channel current/transconductance exhibited a progressive increase while the threshold voltage exhibited a progressive decrease in the OECT response with increasing the alkali metal ionic size. For instance, for OECT with W/L = 500/20 geometries, the maximum transconductance values were g_{max} = 11.9, 14.1 and 22.3 mS, the threshold voltage values were V_{th} = 0.31, 0.27 and 0.20 V, and the figure of merit values were µC* = 3.51, 4.81 and 7.31 F. $cm^{-1}.V^{-1}.s^{-1}$, for LiTFSI, NaTFSI and KTFSI 0.1 M, respectively. In addition, the OECT response yielded excellent sensitivity for alkali metal counterions using secondary electrolytes such as LiCl, NaCl and KCl in a broad range of concentrations from 10 to 1000 mM. We evidence that these P3HT-based OECT devices can be extremely useful to determinate Li^+, Na^+ and K^+ working in the accumulation mode exhibiting sensitivities ranging from $\Delta(-I_{ds})$ = -0.3 to -1.3 mA, -0.6 to -2.2 mA, -2.3 to -4.5 mA and in the case of Li^+, Na^+ and K^+, respectively. This indicates that the cation expulsion mechanism can be used for the indirect sensing of alkali metal ions in P3HT-based OECT devices working in the accumulation mode yielding excellent response compared with those typically observed for PEDOT:PSS-based OECT devices working in the depletion mode.

Keywords: OECT, P3HT, alkali metal counterion, accumulation mode, indirect sensing.

1. Introduction

Organic electrochemical transistors (OECTs) are one of the most promising biosensor devices that can operate in aqueous electrolytes and are particularly interesting for transducing and amplifying low-amplitude ionic fluctuations of biological origin.[1] In an OECT device, the gate electrode controls the amount of current flowing in the channel, which is connected to the gate electrode through an electrolyte. The channel is typically made of an organic mixed conductor that can undergo reversible doping state changes due to its interaction with ionic species present in an aqueous electrolyte. One of the most frequent materials used as a channel for OECTs is the p-type organic semiconductor poly(3,4-ethylenedioxythiophene) doped with poly(styrenesulfonate) (PEDOT:PSS), which allows OECTs to operate in depletion mode, *i.e.* the positive biasing of the gate electrode injects cations into the conducting polymer and there is a flux of ions to provide charge compensation leading to a decrease in the channel current due to the de-doping effect.[2-11] However, it is also possible to operate OECTs in accumulation mode, *i.e.* the negative biasing of the gate electrode injects anions into the conducting polymer, leading to an increase in the channel current.[12] In the latter case, the typical mixed conductor used for this purpose is poly(3-hexylthiophene) (P3HT) and all its glycolated side chain analogs.[12] Although a lot of efforts have been made, up to now, little is known about how dopant ions are injected, transported and transferred as electronic charges in these polymer mixed conductors. Particularly, the use of P3HT without glycolated side chain modification as channel materials is usually reserved for electrolyte-gated organic field-effect transistors (EGOFET) rather than an OECT, considering its hydrophobic nature.[13-18] However, although P3HT swelling abilities are limited compared to its glycolated side chain analogs, there are a lot of studies suggesting that charge transport and transfer processes are far from being only a simple interface phenomenon. For instance, Guardado *et al.* have revealed changes in the crystalline structure of P3HT induced by ionic liquid-mediated electrochemical doping.[19] On the other hand, Giridharagopal *et al.* have shown that amorphous regions of a P3HT film undergo subnanometer swelling as dopant anions from an aqueous electrolyte penetrate the film.[20] Flagg *et al.* have observed that the anion type affects both the transistor current and the threshold voltage, with larger molecular anions resulting in lower threshold voltages and greater transistor currents.[21] In addition, they have also evidenced that smaller anions such as fluoride (F^-), chloride (Cl^-) and bromide (Br^-) enter the polymer film with a

solvation shell of water while the larger anions such as hexafluorophosphate (PF_6^-) and bis(trifluoromethanesulfonyl)imidate ($TFSI^-$) enter the film with little or no water at all.[21] Then, Savva *et al.* have shown that the hydration properties of the dopant can be modulated by simply changing the electrolyte concentration, evidencing an optimum degree of hydration for efficient electrochemical doping in aqueous electrolytes as well as for fast and high gain accumulation mode OECTs.[22] Flagg *et al* have also recently shown that the doping mechanism of OECT based on a polythiophene derivative working in the accumulation mode is not only sensitive to anions but also to the cation counterions.[23] They have proposed a mechanism based on the hydration of the neutral film by electrolyte, followed by cation expulsion from the film upon initial application of an oxidative bias, and then followed by anion injection into the film at higher doping levels.[23] Nonetheless, up to now, there have been only a few reports focused on shedding some light on the structural and molecular aspects of ionic-electronic interactions in polythiophene systems. For instance, the doping mechanism of P3HT using one of the most popular and effective dopants; *i.e.* lithium bis(trifluoromethanesulfonyl)imidate (LiTFSI), has been addressed using static and dynamic DFT simulations.[24,25] In the later reports, it has been evidenced that the alkali metal cation interacts strongly with thiophene rings and the $TFSI^-$ anion/dopant prefers to locate on the P3HT side chain surroundings with its doping ability being more effective for crystalline regions.[24,25] In the present report, we show that the alkali metal counterion can have a non-subtle effect that can be indirectly sensed using P3HT-based OECT devices working in the accumulation mode with bis(trifluoromethanesulfonyl)imidate salts aqueous solution as electrolytes. We have also performed *in-operando* X-ray and Raman scattering studies to provide insights into this interesting behavior. Finally, we have also evaluated the OECT responses depending on the alkali metal counterion in both output and transfer characteristics in the presence of secondary electrolytes such as alkali metal chloride salts.

2. Methodology

2.1 Preparation of OECT devices

The OECT devices with coplanar geometry were prepared as follows: thin gold gate, source and drain electrodes were sputtered onto a glass substrate in a 0.2 mbar argon atmosphere

at 30 mA DC sputtering ion current for 300 s using a removable insulating polymeric template (Scotch® Magic™ Tape 810HK) defining a channel area with length L ~ 20 µm and widths W ~ 1000 or 500 µm. Then, three parts of 2 µL (total 6 µL) of P3HT (SIGMA-ALDRICH CAS 104934-50-1: regioregular > 90%, average M_w 50.000–75.000) dissolved in toluene with 10 mg/ml concentration was deposited on the channel area, spin coated at 1500 rpm for 1 minute and dried at 100 ℃ for 60 minutes yielding a thickness d ~ 2 µm. The same insulating polymer mask was then deposited, leaving only the channel and gate area exposed to LiTFSI, NaTFSI and KTFSI 0.1 M aqueous electrolyte solutions. The electrolyte concentration for each solution was corroborated with conductivity measurements using calibrated instrumentation and data reported in the literature.[26] We also evaluate the addition of LiCl, NaCl and KCl aqueous secondary electrolyte solutions to sense Li^+, Na^+ and K^+ counterions at different concentrations, as well as interference and compensation effects. All the electrolyte salts were provided by SIGMA-ALDRICH and used without prior purification. Finally, not only bare gold but also silver ink-coated gold prepared using SIGMA-ALDRICH silver ink was tested and compared as gate electrodes. A pictorial schematization of the OECT device's preparation and *in-operando* characterization is depicted in **Figure 1a**.

2.2 Characterization of OECT devices

In-operando X-ray scattering profiles were collected for OECT devices using Rigaku Miniflex working with CuKα radiation in the 2θ = 3 – 22˚range with a 0.02˚step in a Bragg-Brentano configuration. *In-operando* microRaman scattering and imaging profiles were collected for OECT devices using WITec alpha300 RA working with 532 nm laser wavelength and < 5 mW laser power in the 60 – 4000 cm^{-1} range with a 1 cm^{-1} resolution in a 15 µm width × 20 µm height cross-section with ~ 300 nm pixel resolution. In both cases, the data were collected directly over the OECT channel covered with a 5 µL drop of electrolyte solution by applying selected gate voltages between the gate and short-circuited source-drain electrodes (V_g = -0.8 and 0.0 V), as depicted in **Figure 1b and 1c**.

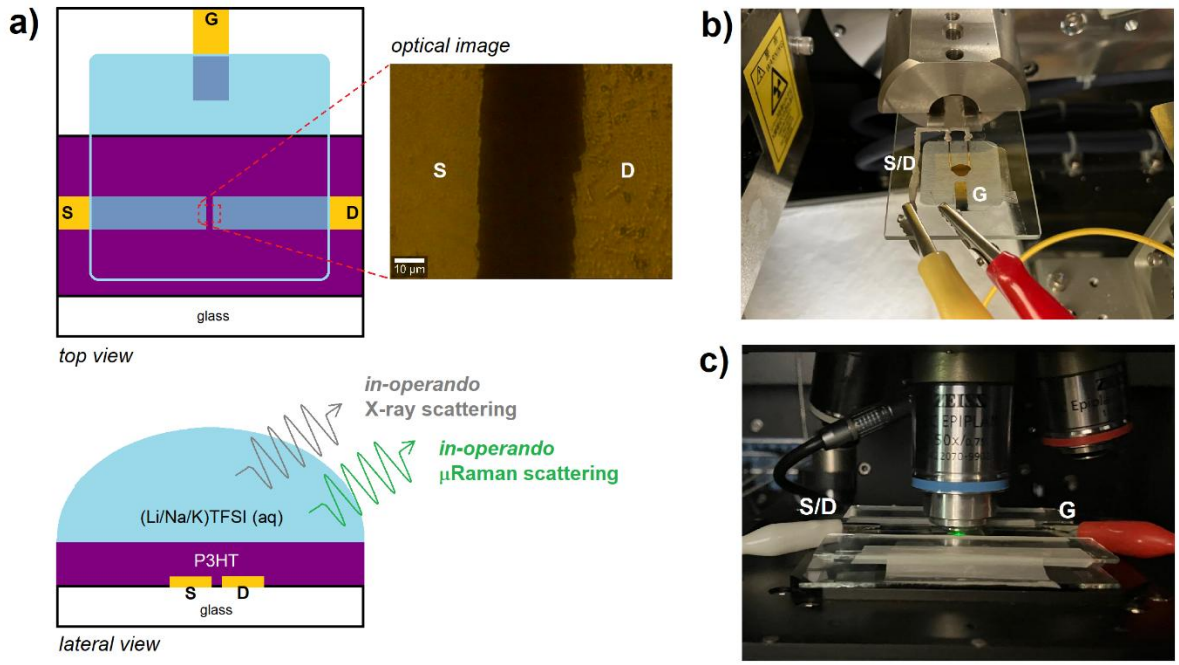

Figure 1 – **a)** Pictorial schematization of OECT device features including an optical image of the channel, **b)** X-ray and **c)** microRaman scattering instrumentation set-up for *in-operando* measurements collected directly over the OECT channel working at selected gate voltages (*i.e.* V_g = 0.0 V and V_g = -0.8 V) with a 5 µL drop of electrolyte solution and without electrolyte.

The inclusion of this particular amount of electrolyte solution was found to be optimal, allowing us to obtain appropriate X-ray and microRaman scattering data, *i.e.* lower amounts lead to electrolyte drying and salt precipitation, while higher amounts lead to quite low scattering intensities due to the excess of aqueous media. Impedance spectroscopy data were also collected between the gate and short-circuited source-drain electrodes of the OECT devices using Gamry Reference 3000 galvanostat/potentiostat working with an AC voltage amplitude of $V_{g,ac}$ = 20 mV in the 0.01 Hz – 1 MHz frequency range and $V_{g,dc}$ = -0.8 to 0.0 V. The channel current (I_{ds}) for our OECT devices was collected between the source and drain electrodes in the V_{ds} = -0.8 V – 0.0 V drain-source voltage range and different applied gate voltages between the gate and the source electrodes in the V_g = -0.8 to 0.0 V range using the Keithley 2450 source-meter. In each case, the gate and source-drain voltages were applied for 5 minutes before each measurement and then each output data was collected for 5 minutes in triplicate (*i.e.* three different devices and electrolyte solutions). Both bare gold and silver ink-coated gold were tested as gate electrodes and, although these are not reference

electrodes, they are still frequently used as gate electrodes in OECTs with coplanar geometry [27,28] and exhibit a broad stability window in LiTFSI electrolyte solutions.[29,30] We evidence a decrease in absolute values and an increment in the standard deviation for the channel current and transconductance values in the case of OECT with lower W/L geometries, as depicted in **Figure S1**. However, the typical shift of maximum channel current and transconductance towards lower gate voltages observed for the case of OECT with lower W/L geometries is quite relevant to work at lower (and thus "safer") voltages. This behavior is typically observed for OECT devices and it is purely ascribed to the geometry of the OECT devices.[31] The OECT output and transfer characteristics were also studied using [LiTFSI] 0.1M + LiCl 10 mM, [LiTFSI] 0.1M + LiCl 100 mM, [LiTFSI] 0.1M + LiCl 1000 mM, [NaTFSI] 0.1M + NaCl 10 mM, [NaTFSI] 0.1M + NaCl 100 mM, [NaTFSI] 0.1M + NaCl 1000 mM, [KTFSI] 0.1M + KCl 10 mM, [KTFSI] 0.1M + KCl 100 mM and [KTFSI] 0.1M + KCl 1000 mM binary electrolyte solutions. In addition, interference and compensation effects were evaluated using [(Li/Na)(TFSI+Cl)] 0.1M, [(Li/K)(TFSI+Cl)] 0.1M and [(Na/K)(TFSI+Cl)] 0.1M binary electrolyte solutions.

3. Results and Discussion

3.1 Structural and chemical characterization of OECT devices

In-operando X-ray scattering profiles collected directly over the OECT channel covered with a 5 µL drop of electrolyte solution at selected gate voltages (*i.e.* V_g = 0.0 V and V_g = -0.8 V) and without electrolyte (*i.e.* exposed to air) are shown in the upper panel of **Figure 2**. The typical P3HT (100) Bragg reflection is observed in all cases, but the other P3HT lower-intensity diffraction peaks are absent due to the relatively small dimension of the OECT channel and the relatively short collection times (~ 7 minutes) used to avoid the electrolyte solution drying and salt precipitation on the OECT channel. The diffraction peaks associated with silver and gold present in the electrodes are absent for $2\theta < 22^{\circ}$values (**Figure S2**) and only a strong diffraction peak is observed at $2\theta \sim 38^{\circ}$associated with the Ag (111) and Au (111) Bragg reflections (not shown in **Figure S2**). It is important to note that the marked decrease in the P3HT (100) Bragg reflection diffraction intensity in the presence of the electrolyte solution is mainly due to the X-ray absorption of the aqueous medium.

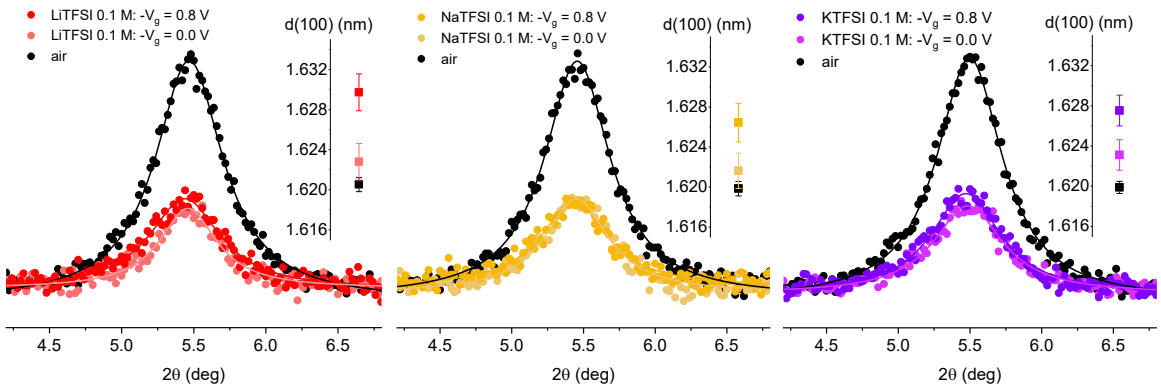

Figure 2 - *In-operando* X-ray scattering profiles collected directly over the OECT channel working at selected gate voltages (*i.e.* V_g = 0.0 V and V_g = -0.8 V) with a 5 µL drop of electrolyte solution and without electrolyte (*i.e.* exposed to air), including peak fit of the P3HT (100) Bragg reflection and corresponding d-spacing values.

However, interesting features can be observed for the P3HT (100) Bragg reflection 2θ position and corresponding d-spacing (typically known as the lamellar spacing), as depicted in the lower panel of **Figure 2**. The lamellar d-spacing for P3HT without exposure to the electrolyte solution was ~ 1.620 nm and it is related to the spacing between P3HT backbones perpendicular to the π-π stacking distance in the crystalline regions.[24] An increase in the lamellar d-spacing of P3HT is observed when embedded with the electrolyte solution at V_g = 0.0 V (up to ~ 1.622-1.623 nm) and further increases at V_g = -0.8 V (up to ~ 1.627-1.629 nm). This evidence shows that the P3HT swelling effect is enhanced when more hydrated ions are injected into the channel, as already observed in the literature.[23] In addition, our results also suggest that the injection of TFSI- anions not only reached the swollen amorphous regions but also the crystalline regions of P3HT. It is important to note that no significant variations were observed between X-ray diffraction pattern replicates. However, although a marked trend in the d-spacing shifts was observed for all cases with acceptable statistical fitting errors, their maximum corresponding Bragg angle shifts (*e.g.* Δd ~ 0.006–0.010 nm corresponds to Δθ ~ 0.02–0.03˚) are slightly above the instrumental resolution (0.02˚ step). *In-operando* microRaman scattering and imaging collected directly over the OECT channel covered with a 5 µL drop of electrolyte solutions at selected gate voltages (*i.e.* V_g = 0.0 V and V_g = -0.8 V) and without electrolyte (*i.e.* exposed to air) are shown in the upper panel of **Figure 3**.

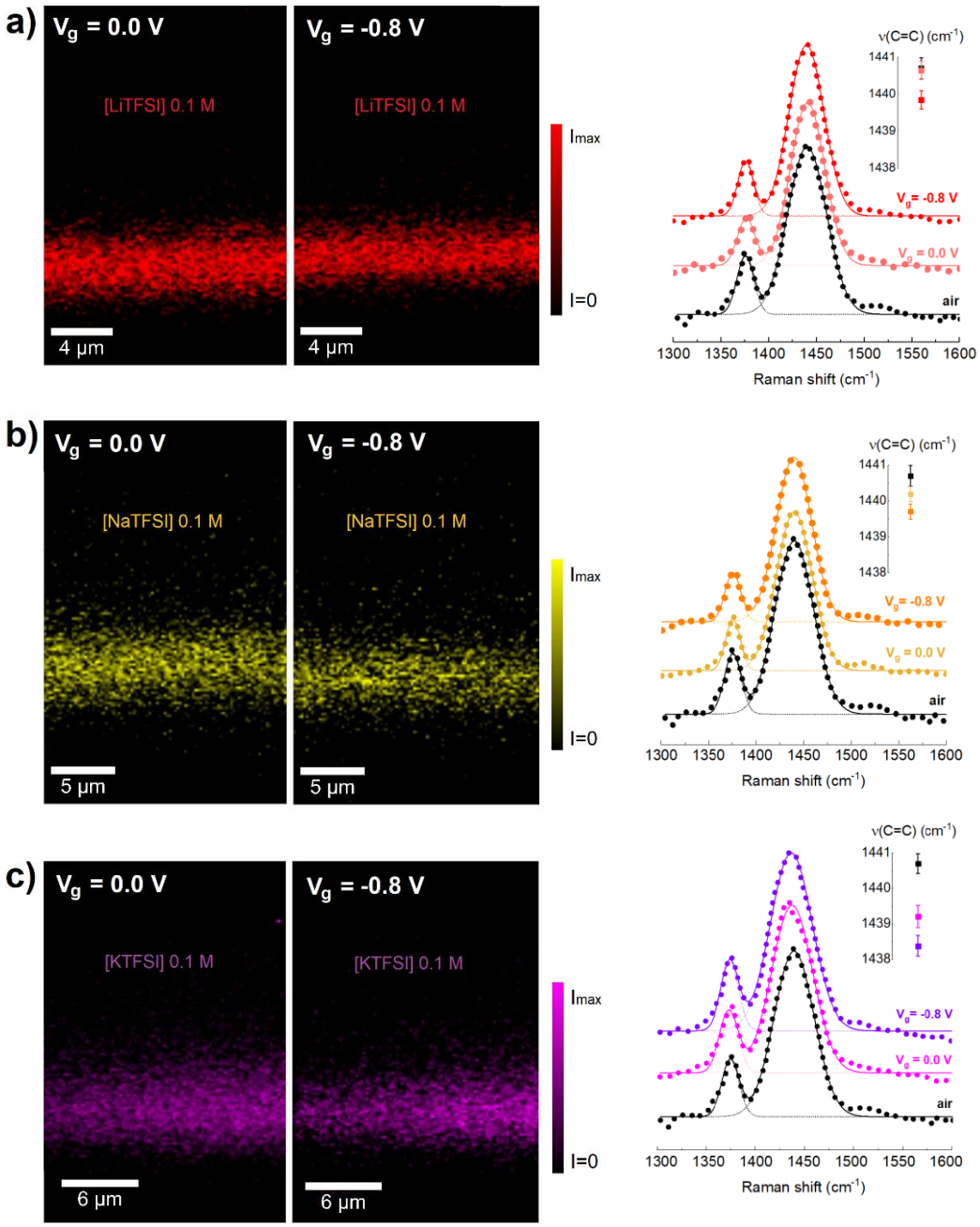

Figure 3 - *In-operando* microRaman imaging profiles collected directly over the OECT channel working at selected gate voltages (*i.e.* V_g = 0.0 V and V_g = -0.8 V) without electrolyte (*i.e.* exposed to air) and with a 5 µL drop of **a**) LiTFSI 0.1 M, **b**) NaTFSI 0.1 M and **c**) KTFSI 0.1 M electrolyte solution (**left panel**). Peak fit of the P3HT thiophene C=C stretching mode and corresponding Raman shift values (**right panel**).

The most relevant vibrational mode associated with P3HT, *i.e.* the thiophene C=C stretching mode at ~ 1440-1438 cm^{-1}, was selected to create the microRaman imaging profiles shown in the left panel of **Figure 3**.[24] The P3HT swollen films are ~ 4 µm wide maintaining their homogeneity even at the interface with the electrolyte solution for all cases. However,

interesting features can be observed for the P3HT thiophene C=C stretching mode and corresponding Raman shift values, as depicted in the right panel of **Figure 3**. A shift towards lower wavenumbers is observed for the thiophene C=C stretching mode at ~ 1440.7 cm^{-1} when embedded with the electrolyte solution at V_g = 0.0 V (down to ~ 1440.6, 1440.1 and 1439.2 cm^{-1}) and further decreases at V_g = -0.8 V (down to ~ 1439.9, 1439.8 and 1438.3 cm^{-1}) for LiTFSI, NaTFSI and KTFSI 0.1 M, respectively. The P3HT thiophene C=C stretching mode shifts toward lower wavenumbers when doped is well-known to be associated with the formation of charge carriers in the thiophene rings.[24] In addition, we observe no relevant variations in the later Raman peak FWHM (~ 43-47 cm^{-1}) for all cases and thus we can not evidence modifications associated with the degree of crystallinity of P3HT.[32,33] Our *in-operando* microRaman spectroscopy studies evidence that the charge transfer through the $TFSI^-$ doping of P3HT [evaluated using the ν(C=C) position (ν) and redshift (Δν)] takes place at V_g = 0.0 V and it is enhanced at V_g = -0.8 V corroborating the accumulation mode configuration, being more pronounced with increasing the alkali metal counterion size. In addition, microRaman imaging at selected regions (P3HT-electrolyte and P3HT-glass) corroborates that the doping process takes place at the P3HT-electrolyte but also at the P3HT-glass (although to a lesser extent) regions and the depth of doping [evaluated using the ν(C=C) position (ν) and redshift (Δν)] is enhanced following $Li^+ < Na^+ < K^+$, as depicted in **Figure S3**. It is important to remark that no significant variations were observed between Raman spectra replicates. However, although a marked trend in the Raman peak shifts was observed for all cases with acceptable statistical fitting errors, their maximum wavenumber shifts (*e.g.* Δν ~ 0.7–1.8 cm^{-1}) are comparable to the instrumental resolution (~ 1.0 cm^{-1}).

3.2 Electrical characterization of OECT devices

To provide insights into the ionic injection and ionic-electronic charge transfer properties of these P3HT-based OECT devices, we performed impedance spectroscopy studies. The total impedance response is defined as:

$$Z = Z' - iZ''$$

where Z' is the real part and Z" is the imaginary part of impedance, respectively. The Nyquist plots (-Z" vs. Z') and the total capacitance as a function of frequency, estimated using the following equation:

$$C(f) = 1/(2\pi f|Z''|)$$

at $V_{g,dc}$ = 0.0 V, are depicted in the left and right panels of **Figure 4**, respectively. The corresponding Bode plots (impedance modulus |Z| and phase (ϕ) vs. f) are depicted in **Figure S4**. The impedance spectroscopy data are quite similar to the typical impedance response observed for OECT devices[34], with some interesting features that will be discussed in the following lines. The volumetric capacitance (C*) can be estimated from the plateau observed at low frequencies for the total capacitance response but, in our case, the presence of a small deviation at low frequencies indicates a non-ideal behavior which is more appropriate to study using a circuit model fitting.[34] Our impedance data showed best fitting with a circuit model based on a resistor (R_{ion}) (representing the electrolyte transport in solution) connected in series with the parallel combination of resistor – diffusive-like constant phase element and capacitive-like constant phase element (R_{ct}//CPE) (representing the electrolyte diffusion and charge transfer processes). An additional parallel combination of resistor and capacitive-like constant phase element (R'_{ion}//CPE'_{ion}) (representing a second electrolyte transport process) was needed to fit the OECT working with LiTFSI and NaTFSI 0.1 M electrolyte solutions, as depicted in **Figure S5**.

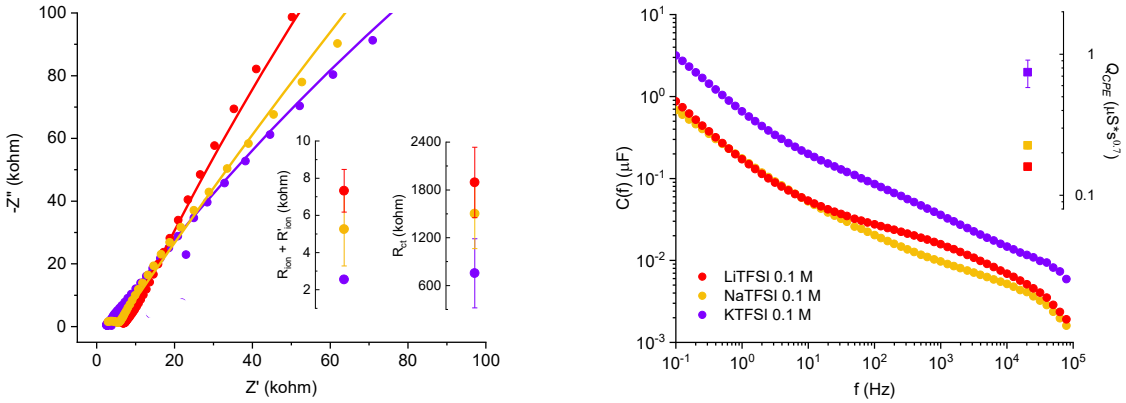

Figure 4 - Nyquist plots including an inset with R_{ion}+R'_{ion} and R_{ct} fitted values (**left panel**) and total capacitance C(f) as a function of frequency, including an inset with Q_{CPE} fitted values (**right panel**) for P3HT-based OECTs working in the accumulation mode with LiTFSI, NaTFSI and KTFSI 0.1M electrolyte solutions.

The constant phase element (CPE) impedance can be described by the following equation:

$$Z_{CPE} = (1/Q)/(i\omega)^{\alpha}$$

where Q (admittance at ω = 1 rad/s) and α (exponent) are frequency-independent parameters, with α = 1 and 0 representing an ideal capacitor and resistor, respectively, while α = 0.5 is associated with diffusion processes.[35] The fitted total ionic resistance (R_{ion} + R'_{ion}) values were 2.6, 5.2 and 7.3 kΩ for KTFSI, NaTFSI and LiTFSI 0.1 M electrolyte solutions, respectively. Here, while R_{ion} can be ascribed to ionic transport in solution as it follows an expected behavior[36], R'_{ion} can be similarly associated with the transport of Na^+ and Li^+ highly hydrated cations through the P3HT polymeric structure. The fitted charge transfer resistance (R_{ct}) values were 755, 1502 and 1895 kΩ for KTFSI, NaTFSI and LiTFSI 0.1 M electrolyte solutions, respectively. On the other hand, the capacitive-like constant phase element (Q_{CPE}) associated with the volumetric capacitance values were 0.75, 0.22 and 0.16 μS.s^{α} with α ~ 0.7 for KTFSI, NaTFSI and LiTFSI 0.1 M electrolyte solutions, respectively. The goodness of fit yielded values of χ^2 = 0.067, 0.005 and 0.001 for KTFSI, NaTFSI and LiTFSI 0.1 M electrolyte solutions, respectively. The non-ideal capacitive process associated volumetric capacitance, estimated as $C = Q_{CPE}(2\pi f_{max}'')^{\alpha-1}$, [37] yielded corresponding volumetric capacitance C* = 21.5, 6.25 and 4.50 $F.cm^{-3}$ values for KTFSI, NaTFSI and LiTFSI 0.1 M electrolyte solutions, respectively. The impedance spectroscopy was also performed at $-V_{g,dc}$ up to 0.8 V, but no drastic variations were observed for R_{ion} + R'_{ion} and R_{ct}, while a slight decrease in the Q_{CPE} was observed with increasing $-V_{g,dc}$ voltages, as depicted in **Figure S6**. In summary, both R_{ct} and Q_{CPE} trends indicate that the charge transfer process and the non-ideal capacitance are enhanced for heavier alkali metal cations, but these results will be discussed later. The output characteristics for P3HT-based OECTs working in the accumulation mode with LiTFSI, NaTFSI and KTFSI 0.1M electrolyte solutions are shown in **Figure 5**. It is well-known that the charge transport/transfer mechanism for these P3HT-based OECT devices working in the accumulation mode is based on the increase in the channel current ($-I_{ds}$) due to the injection of $TFSI^-$ anion dopant in the channel upon the application of negative gate voltages ($-V_g$) [21-23]. However, we also observe distinctive features depending on the alkali counterion of the electrolyte solutions. We evidence a decrease in absolute values for the channel's current and transconductance values, as well as a shifting of their maximum values towards lower $-V_g$ values in the case of OECT with lower W/L geometries.

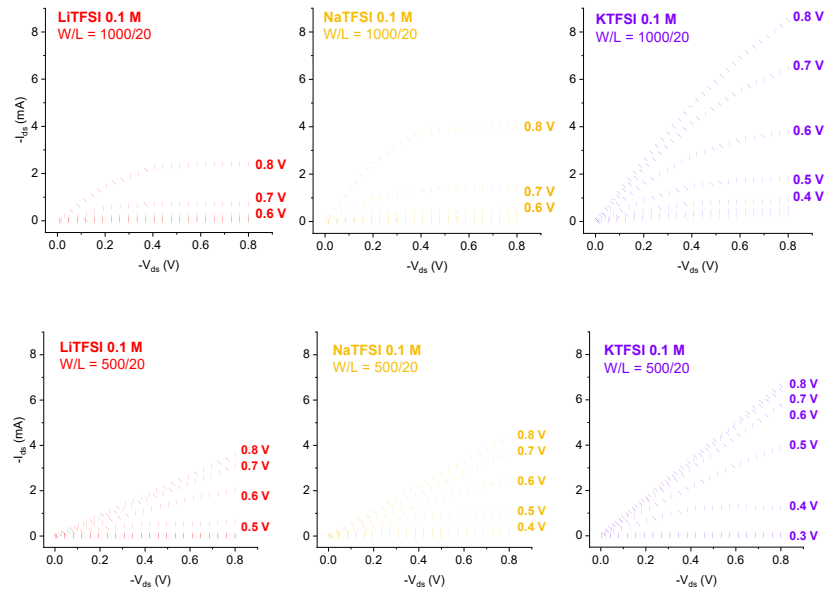

Figure 5 - Output characteristics for OECTs with P3HT-based channel with W/L = 1000/20 and 500/20 working in the accumulation mode with LiTFSI, NaTFSI and KTFSI 0.1M electrolyte solutions.

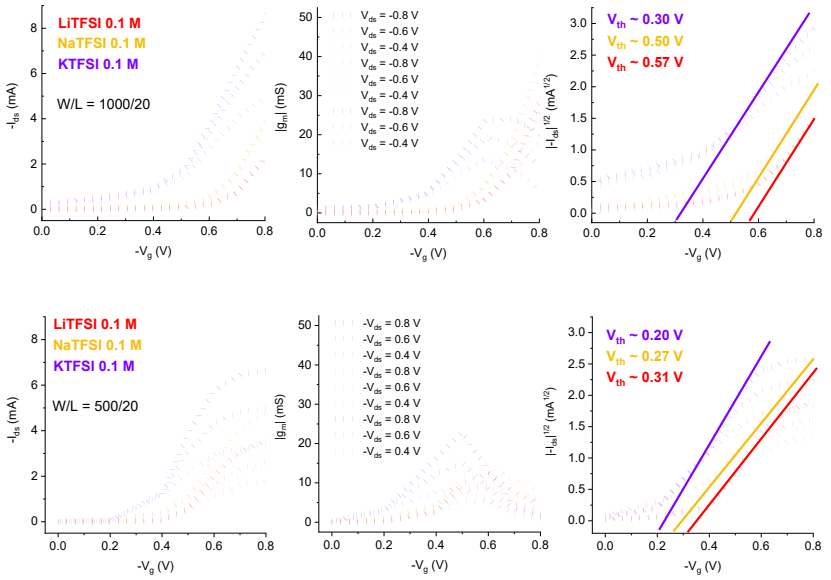

Figure 6 - Transfer characteristics showing channel current ($-I_{ds}$) (**left panels**), transconductance (g_m) (**middle panels**) and square root channel current ($|I_{ds}|^{1/2}$) (**right panels**) for OECTs with P3HT-based channel with W/L = 1000/20 and 500/20 working in the accumulation mode with LiTFSI, NaTFSI and KTFSI 0.1 M electrolyte solutions.

This behavior is typically observed for OECT devices and it is purely ascribed to the geometry of the OECT devices.[31] The output characteristic of OECTs with W/L = 1000/20 showed saturation of $-I_{ds}$ between $-V_{ds}$ = 0.4–0.8 V at the whole gate voltage regime, but OECTs with

W/L = 500/20 evidenced a small deviation at $-V_g$ = 0.6–0.8 V. For both geometries, at given V_{ds} and V_g voltages, the channel current varied following the trend $|I_{ds,KTFSI}| > |I_{ds,NaTFSI}| > |I_{ds,LiTFSI}|$, as shown in **Figure 5**. The transfer characteristics for P3HT-based OECTs working in the accumulation mode with LiTFSI, NaTFSI and KTFSI 0.1M electrolyte solutions are shown in **Figure 6**. The ON/OFF ratios (estimated using the $-I_{ds,-Vg=0.8V}/-I_{ds,-Vg=0.0V}$ ratio) observed for the W/L = 500/20 geometry exhibited 1803, 806 and 1003 values for KTFSI, NaTFSI and LiTFSI 0.1 M electrolyte solutions, respectively. However, although the same apparent trend was observed for the W/L = 1000/20 geometry, the saturation is not fully observed in this transfer curve. The transconductance (g_m) defined as $g_m = |\partial I_{ds}/\partial V_g|$ clearly indicates that the g_m maximum (g_{max}) is shifted towards higher $-V_g$ values for lighter alkali metal counterions, as depicted in the middle panels of **Figure 6**. The maximum normalized transconductance ($g_{max}^* = g_{max}L/Wd$) exhibited g_{max}^* = 2.2, 1.5 and 1.2 $S.cm^{-1}$ for KTFSI, NaTFSI and LiTFSI 0.1 M electrolyte solutions, respectively. However, although the same trend was observed for the W/L = 1000/20 geometry, their corresponding values exhibited slightly higher g_{max}^* values. Finally, for both geometries, the threshold voltage (V_{th}) also showed the same trend, *i.e.* a shifting towards higher $-V_g$ values for lighter alkali metal counterions. For instance, the threshold voltages observed for the W/L = 500/20 geometry exhibited $-V_{th}$ = 0.20, 0.27 and 0.31 V values for KTFSI, NaTFSI and LiTFSI 0.1 M electrolyte solutions, respectively. However, although the same trend was observed for the W/L = 1000/20 geometry, their corresponding values exhibited a shift to higher $-V_{th}$ values. The channel electronic charge carrier mobility (μ) estimated using the Bernard's model equation were 0.34, 0.77 and 0.78 $cm^2.V^{-1}.s^{-1}$ and the μC* figure of merit values were 7.31, 4.81 and 3.51 F. $cm^{-1}.V^{-1}.s^{-1}$, for KTFSI, NaTFSI and LiTFSI 0.1 M electrolyte solutions, respectively. In summary, independently of the geometry dimensions, the increase of the alkali metal counterion's neat size yielded an increase in the channel current and transconductance, as well as a decrease in the threshold voltage. The most relevant OECT parameters discussed earlier are summarized in **Table 1**. As we mentioned earlier, it is well understood that P3HT-based OECT devices working in the accumulation mode are mainly given by the ejection of the counterion (*e.g.* K^+, Na^+ and Li^+) out of the channel towards the electrolyte solution followed by the injection of dopant (*e.g.* $TFSI^-$) into the channel [21-23].

Table 1 – Most relevant P3HT-based OECT parameters working with LiTFSI, NaTFSI and KTFSI 0.1 M electrolytes						
	R_{ion} / R_{ct} (kΩ)	C* ($F.cm^{-3}$)	µC* ($F.cm^{-1}.V^{-1}.s^{-1}$)	ON/OFF ratio	g_{max}* ($S.cm^{-1}$)	V_{th} (V)
Li^+	7.3 / 1895	4.50	3.51	1003	1.2	-0.31
Na^+	5.2 / 1502	6.25	4.81	806	1.5	-0.27
K^+	2.6 / 755	21.5	7.31	1803	2.2	-0.20
These parameters are associated with P3HT-based OECT devices with a W/L = 500/20 geometry and were estimated as detailed in the manuscript.						

However, our data suggests that the cation expulsion is strongly alkali metal counterion dependent and has a significant effect on the performance of P3HT-based OECT devices working in the accumulation mode. To confirm the alkali metal counterion effect, we also show the output and transfer characteristics of OECT devices working with KTFSI, NaTFSI and LiTFSI 0.1 M primary electrolytes interacting with KCl, NaCl and LiCl secondary electrolytes at different concentrations ranging from 10 to 1000 mM, as depicted in **Figure 7** and **8**. Here, we are keeping constant the $TFSI^-$ dopant concentration but increasing the alkali metal counterion concentration using chloride salts, which are known to have almost quite low doping ability and thus almost no response on these OECTs in the $-V_g$ = 0.0 to 0.8 V range [21-23]. The alkali metal counterion concentration increment led to a decrease in the OECT channel currents at a fixed gate voltage for all cases, being strongly dependent on the nature of the alkali metal counterion, as depicted in **Figure 7**. The transfer characteristics at fixed $-V_{ds}$ = 0.8 V for OECTs with P3HT-based channel working in the accumulation mode with [LiTFSI] 0.1M, [LiTFSI] 0.1M + LiCl 10 mM, [LiTFSI] 0.1M + LiCl 100 mM and [LiTFSI] 0.1M + LiCl 1000 mM, [NaTFSI] 0.1M, [NaTFSI] 0.1M + NaCl 10 mM, [NaTFSI] 0.1M + NaCl 100 mM and [NaTFSI] 0.1M + NaCl 1000 mM, [KTFSI] 0.1M, [KTFSI] 0.1M + KCl 10 mM, [KTFSI] 0.1M + KCl 100 mM and [KTFSI] 0.1M + KCl 1000 mM electrolyte solutions are shown in **Figure 8**. A progressive shift towards higher $-V_g$ values for the maximum current ($-I_{ds}$), maximum transconductance (g_m) and threshold voltage (V_{th}) can be observed with increasing the LiCl, NaCl and KCl salt concentrations, being more pronounced for heavier alkali metal counterions. This confirms that the cation expulsion is an important contribution to the ionic injection mechanism on these OECT devices working in the accumulation mode.

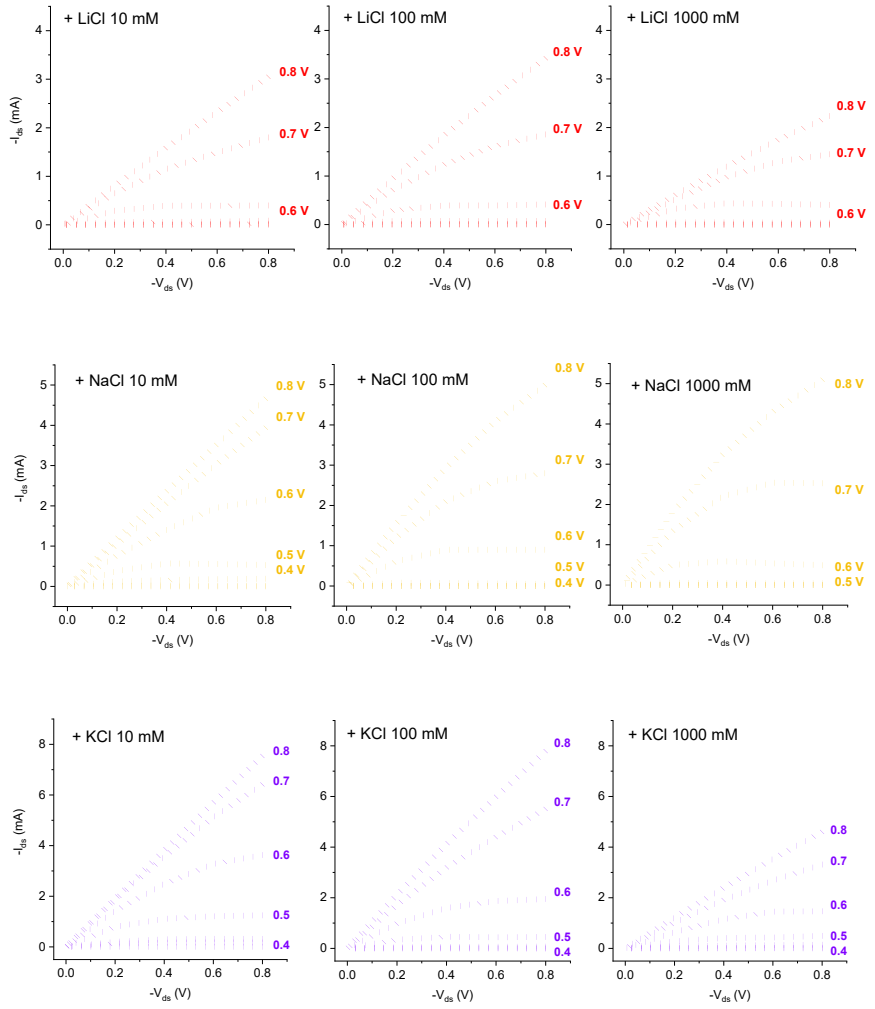

Figure 7 - Output characteristics for P3HT-based OECTs working in the accumulation mode with [LiTFSI] 0.1M + LiCl 10 mM, [LiTFSI] 0.1M + LiCl 100 mM and [LiTFSI] 0.1M + LiCl 1000 mM (**upper panel**), [NaTFSI] 0.1M + NaCl 10 mM, [NaTFSI] 0.1M + NaCl 100 mM and [NaTFSI] 0.1M + NaCl 1000 mM (**middle panel**), [KTFSI] 0.1M + KCl 10 mM, [KTFSI] 0.1M + KCl 100 mM and [KTFSI] 0.1M + KCl 1000 mM (**lower panel**) electrolyte solutions.

The sensitivity for each metal counterion $\Delta(-I_{ds})$ is calculated using the following equation:

$$\Delta(-I_{ds}) = (-I_{ds})_{MTFSI,0.1\ M} - (-I_{ds})_{MTFSI,0.1\ M + MCl,X}$$

with M being Li, Na and K, and X = 10, 100 and 1000 mM. The OECT sensitivity as a function of the alkali metal counterion concentration at $-V_{ds}$ = 0.8 and $-V_g$ = 0.8 V is depicted in **Figure 9**. It is interesting to note that the sensitivity showed a dramatic increment in absolute value for heavier alkali metals following $\Delta(-I_{ds})_{K+} > \Delta(-I_{ds})_{Na+} > \Delta(-I_{ds})_{Li+}$ at a given salt concentration. In addition, the best sensitivity is observed very close to those $-V_g$ values where transconductance was maximum for each case when the secondary electrolytes were absent.

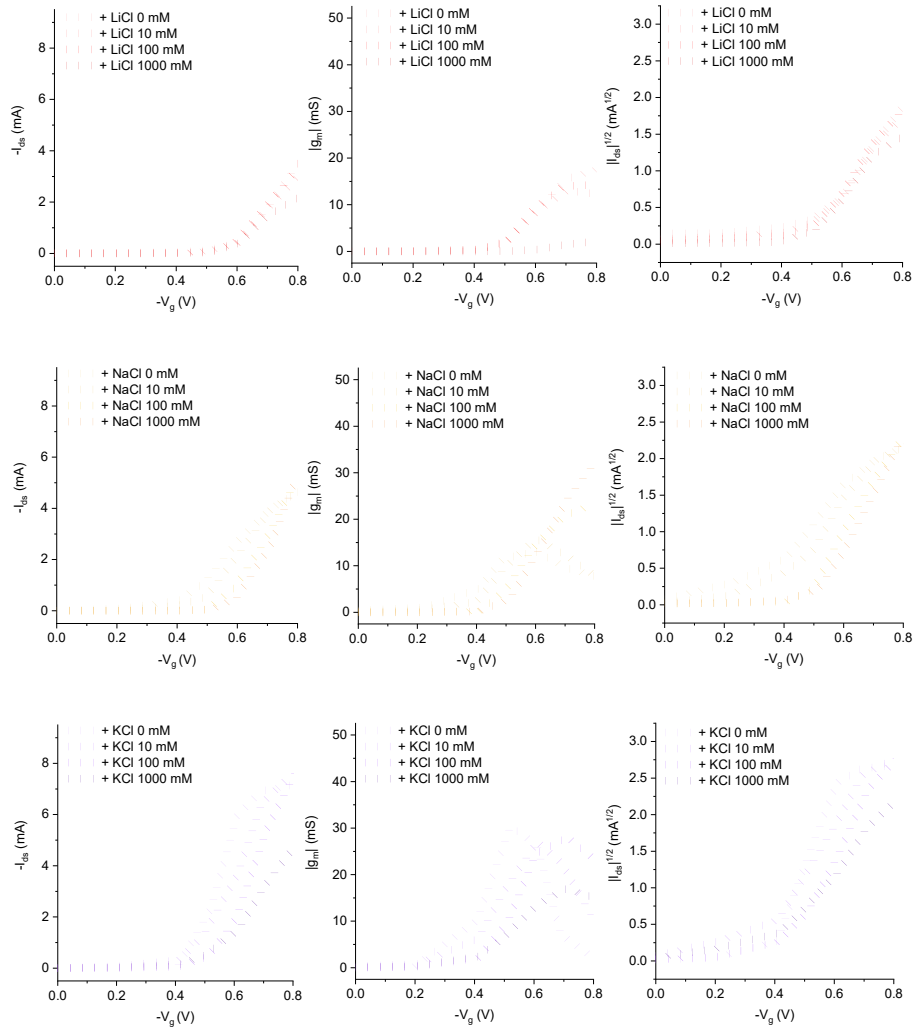

Figure 8 - Transfer characteristics at fixed V_{ds} = -0.8 V showing channel current ($-I_{ds}$) (**left panels**), transconductance (g_m) (**middle panels**) and square root channel current ($|I_{ds}|^{1/2}$) (**right panels**) for OECTs with P3HT-based channel working in the accumulation mode with [LiTFSI] 0.1M, [LiTFSI] 0.1M + LiCl 10 mM, [LiTFSI] 0.1M + LiCl 100 mM and [LiTFSI] 0.1M + LiCl 1000 mM (**upper panel**), [NaTFSI] 0.1M, [NaTFSI] 0.1M + NaCl 10 mM, [NaTFSI] 0.1M + NaCl 100 mM and [NaTFSI] 0.1M + NaCl 1000 mM (**middle panel**), [KTFSI] 0.1M, [KTFSI] 0.1M + KCl 10 mM, [KTFSI] 0.1M + KCl 100 mM and [KTFSI] 0.1M + KCl 1000 mM (**lower panel**) electrolyte solutions.

It is important to note that the channel's current standard deviation, by evaluating OECT devices in triplicate, can be relatively high (*i.e.* ~ 1 mA). Thus, it is noteworthy to mention that the sensitivity for heavier alkali metal ions (*e.g.* K^+, and Na^+ to a lesser extent) is sufficiently high and thus adequate for sensing purposes but starts to be comparable with the replicate's statistical errors for lighter alkali metal ions (*e.g.* Li^+). In conclusion, these P3HT-based OECT devices can be extremely useful to determinate K^+ (and Na^+ to a lesser extent) working in the accumulation mode in a broad range of concentrations from 10 to 1000 mM, exhibiting

sensitivities ranging from $\Delta(-I_{ds})$ = -0.3 to -1.3 mA, -0.6 to -2.2 mA, -2.3 to -4.5 mA for Li^+, Na^+ and K^+, respectively. In the literature, the most typical OECT devices for these purposes are PEDOT:PSS working in the depletion mode, exhibiting comparable current and transconductance values [9,31,38,39]. However, these PEDOT:PSS-based OECT devices usually need the presence of additives (such as ethylene glycol or dimethyl sulfoxide) to achieve high current and transconductance, but on the other hand, these small polar molecules can eventually migrate to the electrolyte after cycling [9,31,38,39]. Finally, we also show the output and transfer characteristics with two different alkali metal counterions to evaluate cation species interference and compensation effects. The OECT transfer characteristic response for the (Li/Na)(TFSI+Cl), (Li/K)(TFSI+Cl) and (Na/K)(TFSI+Cl) is somewhat expected as it falls between the response observed for the Li(TFSI+Cl) and Na(TFSI+Cl), Li(TFSI+Cl) and K(TFSI+Cl), Na(TFSI+Cl) and K(TFSI+Cl), respectively, as depicted in **Figure S7** and **Figure S8**. However, it is important to note that the differences between different binary mixtures of alkali metals responses are less marked compared to their isolated counterparts. For this reason, the sensing of a mixture of cations using these P3HT-based OECT could be quite challenging but of particular interest when comparing the same dopant in the presence of different alkali metal counterions and having a sort of cation-independent response of the OECT for comparison purposes.

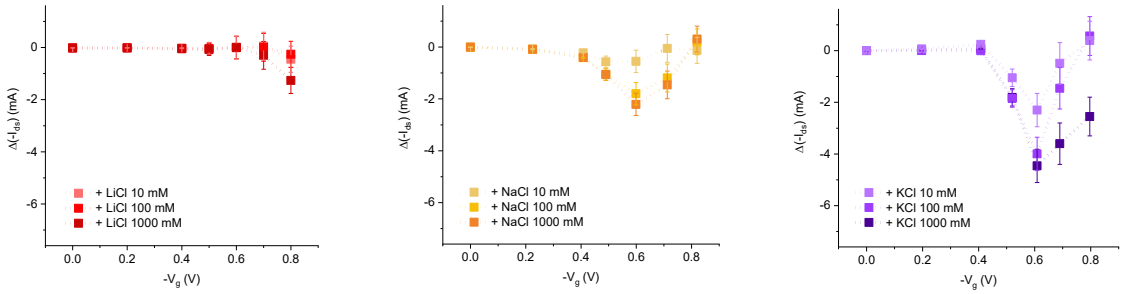

Figure 9 – Sensitivity measured as $\Delta(-I_{ds})$ as a function of salt concentration for OECTs with P3HT-based channel working in the accumulation mode for [LiTFSI] 0.1M + LiCl 10 mM, [LiTFSI] 0.1M + LiCl 100 mM and [LiTFSI] 0.1M + LiCl 1000 mM (**left panel**), [NaTFSI] 0.1M + NaCl 10 mM, [NaTFSI] 0.1M + NaCl 100 mM and [NaTFSI] 0.1M + NaCl 1000 mM (**middle panel**), [KTFSI] 0.1M + KCl 10 mM, [KTFSI] 0.1M + KCl 100 mM and [KTFSI] 0.1M + KCl 1000 mM (**right panel**) electrolyte solutions.

In order to provide some rational explanation for the effect of alkali metal counterions, it is important to keep in mind that the atomic ionic radius follows the inverse trend compared to the hydration ionic radius for alkali metals in aqueous solutions, *i.e.* r_{Li+} (60 pm) < r_{Na+} (95 pm) < r_{K+} (133 pm), and $r_{Li+,H2O}$ (382 pm) > $r_{Na+,H2O}$ (358 pm) > $r_{K+,H2O}$ (331 pm).[36] It is interesting to observe that, contrary to the behavior observed in solution or swollen regions, the mobility of the neat cations through the "dry" polymeric structure should follow the opposite trend if their charge-to-(mass or volume) ratios are only considered. However, other aspects such as the ionic-pair dissociation between these cations and $TFSI^-$ dopant as well as their interaction with the P3HT polymeric structure should also be considered. For instance, we have already reported that the presence of a small alkali metal cation, such as lithium-ion, interacts strongly with the thiophene rings of P3HT interchain space in the crystalline regions. [24,25] Thus, it can be expected that the larger alkali metal cation, such as potassium-ion, can be more easily ejected from the P3HT interchain space due to its large size. A schematization of the charge transport/transfer for P3HT-based OECTs working in the accumulation mode with LiTFSI, NaTFSI and KTFSI 0.1M electrolyte solutions is shown in **Figure 10**. Based on all the previous discussions, we can conclude that the resistance associated with the alkali metal ionic transport in both the aqueous solution and the swollen interface of P3HT follows the trend ($R_{ion,K+}$+$R'_{ion,K+}$) < ($R_{ion,Na+}$+$R'_{ion,Na+}$) < ($R_{ion,Li+}$+$R'_{ion,Li+}$) considering their corresponding hydration ionic radius, as depicted in the upper and middle panel of **Figure 10**. However, the resistance associated with the ionic transport through the "dry regions" of P3HT should follow the opposite trend considering their corresponding atomic ionic radius. Thus, our data suggest that the major contribution to global resistance associated with the ionic transport through the polymer can be mainly explained by considering the transport of hydrated species rather than neat species. On the other hand, the ionic-electronic charge transfer resistance (R_{ct}) associated with the injection of dopant and ejection of alkali metal cations from the P3HT interchain space follows the trend $R_{ct,K+}$ < $R_{ct,Na+}$ < $R_{ct,Li+}$, as depicted in the lower panel of **Figure 10**. Since small alkali metal cation, such as neat lithium-ion, interacts strongly with the thiophene rings of P3HT interchain space of the crystalline regions [24,25], it can be expected that the larger alkali metal cation, such as neat potassium-ion, can be more easily ejected from the P3HT interchain space due to its large size.

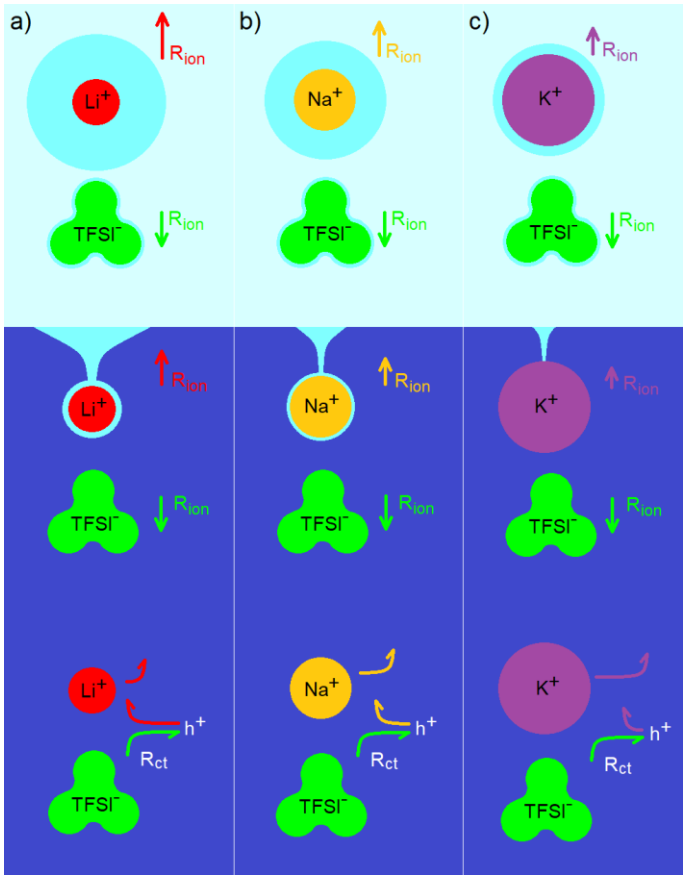

Figure 10 - Schematization of charge transport and transfer for P3HT-based OECTs working in the accumulation mode with **a)** LiTFSI, **b)** NaTFSI and **c)** KTFSI 0.1M electrolyte solutions. The vertical arrows represent ionic transport in the aqueous solution (**upper panel**), in the swollen interface of P3HT (**middle panel**) and the horizontal curved arrows represent the ionic transport and ionic-electronic charge transfer (doping) process in the "dry regions" of P3HT (**lower panel**).

In this scenario, if the cations are more easily ejected and $TFSI^-$ dopant is more dissociated in the channel, the increase in the volumetric capacitance following the observed trend $C^*_{K+} > C^*_{Na+} > C^*_{Li+}$ is expected due to the enhanced anion storage ability of the OMIEC film. In addition, as the $TFSI^-$ doping ability is expected to be enhanced as well, an increase in the channel current is also expected following the trend $|I_{ds,KTFSI}| > |I_{ds,NaTFSI}| > |I_{ds,LiTFSI}|$ at given V_{ds} and V_g voltages but also $\Delta(-I_{ds})_{K+} > \Delta(-I_{ds})_{Na+} > \Delta(-I_{ds})_{Li+}$ at a given salt concentration. Furthermore, in the same scenario, the decrease in $-V_{th}$ values following the observed trend $-V_{th,Li+} > -V_{th,Na+} > -V_{th,K+}$ can be also expected based on the enhanced $TFSI^-$ ion penetration in P3HT films. Finally, it is important to note that although the figure of merit observed trend $\mu C^*_{K+} > \mu C^*_{Na+} > \mu C^*_{Li+}$ is also in agreement with the $TFSI^-$ enhanced dissociation scenario, its major contribution is related to the volumetric capacitance (C*) rather than with the electronic charge carrier mobility (μ). Thus, our studies suggest that the cation expulsion is

strongly alkali metal-dependent and can be used for their indirect sensing in the presence of primary (salt including dopant) and secondary (salt without including dopant) electrolytes.

4. Conclusions

Here, we report the alkali metal counterion effect and their indirect sensing using poly(3-hexylthiophene)-based OECT devices working in the accumulation mode with bis(trifluoromethanesulfonyl)imidate salts aqueous solution as electrolytes. Our studies based on *in-operando* microRaman spectroscopy corroborate the OECT accumulation mode charge injection and transfer processes. In addition, our studies using *in-operando* X-ray scattering indicate that the injection of dopants not only reached the swollen amorphous regions but also the crystalline regions of poly(3-hexylthiophene) (P3HT). Interestingly, we have observed characteristic features depending on the alkali metal counterion in both output and transfer characteristics for these OECT devices. The channel current/transconductance exhibited a progressive increase while the threshold voltage exhibited a progressive decrease in the OECT response with increasing the alkali metal ionic size. For instance, for OECT with W/L = 500/20 geometries, the maximum transconductance values were g_{max} = 11.9, 14.1 and 22.3 mS while the threshold voltage values were $-V_{th}$ = 0.31, 0.27 and 0.20 V, and the figure of merit values were μC^* = 3.51, 4.81 and 7.31 F. $cm^{-1}.V^{-1}.s^{-1}$ for LiTFSI, NaTFSI and KTFSI, respectively. In addition, the OECT response yielded drastic variations when increasing the alkali metal counterion concentration using secondary electrolytes as analytes such as LiCl, NaCl and KCl. We evidence that these P3HT-based OECT devices can be extremely useful to determinate K^+ (and Na^+ to a lesser extent) working in the accumulation mode in a broad range of concentrations from 10 to 1000 mM, exhibiting sensitivities ranging from $\Delta(-I_{ds})$ = -0.3 to -1.3 mA, -0.6 to -2.2 mA, -2.3 to -4.5 mA and in the case of Li^+, Na^+ and K^+, respectively. This indicates that the cation expulsion mechanism can be used for the indirect sensing of alkali metal ions in P3HT-based OECT devices working in the accumulation mode, yielding excellent performance compared with typical PEDOT:PSS-based OECT devices working in the depletion mode.

Supporting Information

Transfer characteristics including standard deviation based on triplicate measurements for OECTs with P3HT-based channel with W/L = 1000/20 (upper panel) and 500/20 (lower panel). In-operando X-ray scattering and microRaman imaging profiles collected directly over the OECT channel working at selected gate voltages. Circuit model used for impedance spectroscopy data fitting, Bode plots data and corresponding fitting curves and Q_{CPE} fitted values as a function of $V_{g,dc}$ voltages. Output and transfer characteristics for P3HT-based OECTs working in the accumulation mode with [(Li/Na)(TFSI+Cl)] 0.1M (upper panel), [(Li/K)(TFSI+Cl)] 0.1M (middle panel), and [(Na/K)(TFSI+Cl)] 0.1M (lower panel) electrolyte solutions.

Author Contributions

The manuscript was written through the contributions of all authors. All authors have given approval to the final version of the manuscript.

Acknowledgments

The authors thank the collaboration of Dr. Ricardo Faccio and the Uruguayan CSIC, ANII, and PEDECIBA funding institutions. We also appreciate the financial support of ANII POS_NAC_2024_1_183297 PhD grant.

References

(1) Kukhta, N. A.; Marks, A.; Luscombe, C. K. Molecular Design Strategies toward Improvement of Charge Injection and Ionic Conduction in Organic Mixed Ionic-Electronic Conductors for Organic Electrochemical Transistors. Chem. Rev. 2022, 122, 4325−4355.

(2) Paulsen, B. D.; Tybrandt, K.; Stavrinidou, E.; Rivnay, J. Organic mixed ionic-electronic conductors. Nat. Mater. 2020, 19, 13−26.

(3) Savva, A.; Hallani, R.; Cendra, C.; Surgailis, J.; Hidalgo, T. C.; Wustoni, S.; Sheelamanthula, R.; Chen, X.; Kirkus, M.; Giovannitti, A.; Salleo, A.; McCulloch, I.; Inal, S. Balancing Ionic and Electronic Conduction for High- Performance Organic Electrochemical Transistors. Adv. Funct. Mater. 2020, 30, 1907657.

(4) Bischak, C. G.; Flagg, L. Q.; Yan, K.; Rehman, T.; Davies, D. W.; Quezada, R. J.; Onorato, J. W.; Luscombe, C. K.; Diao, Y.; Li, C. Z.; Ginger, D. S. A Reversible Structural Phase Transition by

Electrochemically-Driven Ion Injection into a Conjugated Polymer. J. Am. Chem. Soc. 2020, 142, 7434−7442.

(5) Rivnay, J.; Inal, S.; Collins, B. A.; Sessolo, M.; Stavrinidou, E.; Strakosas, X.; Tassone, C.; Delongchamp, D. M.; Malliaras, G. G. Structural Control of Mixed Ionic and Electronic Transport in Conducting Polymers. Nat. Commun. 2016, 7, 11287.

(6) Dong, B. X.; Nowak, C.; Onorato, J. W.; Strzalka, J.; Escobedo, F. A.; Luscombe, C. K.; Nealey, P. F.; Patel, S. N. Influence of Side-Chain Chemistry on Structure and Ionic Conduction Characteristics of Polythiophene Derivatives: A Computational and Experimental Study. Chem. Mater. 2019, 31 (4), 1418−1429.

(7) Onorato, J. W.; Wang, Z.; Sun, Y.; Nowak, C.; Flagg, L. Q.; Li, R.; Dong, B. X.; Richter, L. J.; Escobedo, F. A.; Nealey, P. F.; Patel, S. N.; Luscombe, C. K. Side chain engineering control of mixed conduction in oligoethylene glycol-substituted polythiophenes. J. Mater. Chem. A 2021, 9, 21410−21423.

(8) Rivnay, J.; Inal, S.; Salleo, A.; Owens, R. M.; Berggren, M.; Malliaras, G. G. Organic electrochemical transistors. Nat. Rev. Mater. 2018, 3, 17086.

(9) Khodagholy, D.; Rivnay, J.; Sessolo, M.; Gurfinkel, M.; Leleux, P.; Jimison, L. H.; Stavrinidou, E.; Herve, T.; Sanaur, S.; Owens, R. M.; Malliaras, G. G. High transconductance organic electrochemical transistors. Nat. Commun. 2013, 4, 2133.

(10) Bießmann, L.; Kreuzer, L. P.; Widmann, T.; Hohn, N.; Moulin, J. F.; Müller-Buschbaum, P. Monitoring the Swelling Behavior of PEDOT:PSS Electrodes under High Humidity Conditions. ACS Appl. Mater. Interfaces 2018, 10, 9865−9872.

(11) Romero, M.; Mombrú, D.; Pignanelli, F.; Faccio, R.; Mombrú, A. W. Mixed Ionic-Electronic Transport for PEDOT:PSS-Based Zero-Gated Organic Electrochemical Transistors Using Impedance Spectroscopy and Micro-Raman Imaging. ACS Appl. Electron. Mater. 2023, 5, 9, 4863–4874.

(12) Inal, S.; Rivnay, J.; Leleux, P.; Ferro, M.; Ramuz, M.; Brendel, J. C.; Schmidt, M. M.; Thelakkat, M.; Malliaras, G. G. A High Transconductance Accumulation Mode Electrochemical Transistor. Adv. Mater. 2014, 26 (44), 7450−7455.

(13) Macchia, E.; Manoli, K.; Holzer, B.; Di Franco, C.; Ghittorelli, M.; Torricelli, F.; Alberga, D.; Mangiatordi, G. F.; Palazzo, G.; Scamarcio, G.; Torsi, L. Single-molecule detection with a millimetre-sized transistor. Nat. Commun. 2018, 9, 3223.

(14) Seshadri, P.; Manoli, K.; Schneiderhan-Marra, N.; Anthes, U.; Wierzchowiec, P.; Bonrad, K.; Di Franco, C.; Torsi, L. Low-picomolar, label-free procalcitonin analytical detection with an electrolyte-gated organic field-effect transistor based electronic immunosensor. Biosens. Bioelectron. 2018, 104, 113.

(15) Macchia, E.; Manoli, K.; Holzer, B.; Di Franco, C.; Picca, R. A.; Cioffi, N.; Scamarcio, G.; Palazzo, G.; Torsi, L. Selective single-molecule analytical detection of C-reactive protein in saliva with an organic transistor. Anal. Bioanal. Chem. 2019, 411, 4899.

(16) Macchia, E.; Sarcina, L.; Picca, R. A.; Manoli, K.; Di Franco, C.; Scamarcio, G.; Torsi, L. Ultra-low HIV-1 p24 detection limits with a bioelectronic sensor. Anal. Bioanal. Chem. 2020, 412, 811.

(17) Sarcina, L.; Viola, F.; Modena, F.; Picca, R. A.; Bollella, P.; Di Franco, C.; Cioffi, N.; Caironi, M.; Osterbacka, R.; Esposito, I.; Scamarcio, G.; Torsi, L.; Torricelli, F.; Macchia, E. A large-area organic transistor with 3D-printed sensing gate for noninvasive single-molecule detection of pancreatic mucinous cyst markers. Anal. Bioanal. Chem. 2022, 414, 5657.

(18) Sarcina, L.; Macchia, E.; Loconsole, G.; D'Attoma, G.; Bollella, P.; Catacchio, M.; Leonetti, F.; Di Franco, C.; Elicio, V.; Scamarcio, G.; Palazzo, G.; Boscia, D.; Saldarelli, P.; Torsi, L. Fast and Reliable Electronic Assay of a Xylella fastidiosa Single Bacterium in Infected Plants Sap. Adv. Sci. 2022, 9, 2203900.

(19) Guardado, J. O.; Salleo, A. Structural Effects of Gating Poly(3hexylthiophene) through an Ionic Liquid. Adv. Funct. Mater. 2017, 27 (32), 1701791.

(20) Giridharagopal, R.; Flagg, L. Q.; Harrison, J. S.; Ziffer, M. E.; Onorato, J.; Luscombe, C. K.; Ginger, D. S. Electrochemical strain microscopy probes morphology-induced variations in ion uptake and performance in organic electrochemical transistors. Nat. Mater. 2017, 16, 737.

(21) Flagg, L. Q.; Giridharagopal, R.; Guo, J.; Ginger, D. S. Anion-Dependent Doping and Charge Transport in Organic Electrochemical Transistors. Chem. Mater. 2018, 30 (15), 5380−5389.

(22) Savva, A.; Cendra, C.; Giugni, A.; Torre, B.; Surgailis, J.; Ohayon, D.; Giovannitti, A.; McCulloch,I.; Di Fabrizio, E.; Salleo, A.; Rivnay, J.; Inal, S. Influence of Water on the Performance of Organic Electrochemical Transistors. Chem. Mater. 2019, 31, 927−937.

(23) Lucas Q. Flagg, Connor G. Bischak, Ramsess J. Quezada, Jonathan W. Onorato, Christine. K. Luscombe, and David S. Ginger. P-Type Electrochemical Doping Can Occur by Cation Expulsion in a High-Performing Polymer for Organic Electrochemical Transistors. ACS Materials Lett. 2020, 2, 254−260.

(24) Mombrú, D.; Romero, M.; Faccio, R.; Mombrú, A.W. Unraveling the Lithium Bis(trifluoromethanesulfonyl)imide (LiTFSI) Doping Mechanism of Regioregular Poly(3-hexylthiophene): Experimental and Theoretical Study. J. Phys. Chem. C 2020, 124, 13, 7061–7070.

(25) Mombrú, D.; Romero, M.; Faccio, R.; Mombrú, A.W. Ab Initio Molecular Dynamics Assessment on the Mixed Ionic–Electronic Transport for Crystalline Poly(3-Hexylthiophene) Using Full Explicit Lithium-Based Dopants and Additives. Macromolecules 2022, 55, 1, 113–124.

(26) Lee, S.H.; Rasaiah, J.C. Molecular dynamics simulation of ionic mobility. I. Alkali metal cations in water at 25C. J. Chem. Phys. 1994, 101, 6964-6974.

(27) Tarabella, G.; Santato, C.; Yang, S.Y.; Iannotta, S.; Malliaras, G.G.; Cicoira, F. Effect of the gate electrode on the response of organic electrochemical transistors. Applied Physics Letters 2010, 97, 123304.

(28) Sensi, M.; Berto, M.; Candini, A.; Liscio, A.; Cossarizza, A.; Beni, V.; Biscarini, F.; Bortolotti, C.A. Modulating the Faradic Operation of All-Printed Organic Electrochemical Transistors by Facile in Situ Modification of the Gate Electrode. ACS Omega 2019, 4, 5374−5381.

(29) Coustan, L.; Shul, G.; Bélanger, D. Electrochemical behavior of platinum, gold and glassy carbon electrodes in water-in-salt electrolyte. Electrochemistry Communications 2017, 77, 89–92.

(30) Coustan, L.; Bélanger, D. Electrochemical activity of platinum, gold and glassy carbon electrodes in water-in-salt electrolyte. Journal of Electroanalytical Chemistry 2019, 854, 113538.

(31) Rivnay, J.; Leleux, P.; Sessolo, M.; Khodagholy, D.; Hervé, T.; Fiocchi, M.; Malliaras, G. G. Organic Electrochemical Transistors with Maximum Transconductance at Zero Gate Bias. Adv. Mater. 2013, 25, 7010–7014.

(32) Tsoi, W. C.; James, D. T.; Kim, J. S.; Nicholson, P. G.; Murphy, C. E.; Bradley, D. D. C.; Nelson, J.; Kim, J.-S. The Nature of In-Plane Skeleton Raman Modes of P3HT and Their Correlation to the Degree of Molecular Order in P3HT:PCBM Blend Thin Films. Journal of the American Chemical Society 2011, 133(25), 9834–9843.

(33) Dickson, L. E.; Cranston, R. R.; Xu, H.; Swaraj, S.; Seferos, D. S.; Lessard, B. H. Blade Coating Poly(3-hexylthiophene): The Importance of Molecular Weight on Thin-Film Microstructures. ACS Appl. Mater. Interfaces 2023, 15, 47, 55109–55118.

(34) Ohayon, D.; Druet, V.; Inal, S. A guide for the characterization of organic electrochemical transistors and channel materials. Chem. Soc. Rev., 2023, 52, 1001–1023.

(35) Orazem, M. E.; Tribollet, B. Electrochemical Impedance Spectroscopy; John Wiley & Sons, 2008. Chapter 11, Diffusion Impedance, Pages: 183-210.

(36) Zhong, C.; Deng, Y.; Hu, W.; Qiao, J.; Zhang, L.; Zhang, J. A review of electrolyte materials and compositions for electrochemical supercapacitors. Chem. Soc. Rev., 2015, 44, 7484—7539.

(37) Chang, B.-Y. Conversion of a Constant Phase Element to an Equivalent Capacitor. J. Electrochem. Sci. Technol. 2020, 11, 318–321.

(38) Koutsouras, D. A.; Lieberth, K.; Torricelli, F.; Gkoupidenis, P.; Blom, P. W. M. Selective Ion Detection with Integrated Organic Electrochemical Transistors. Adv. Mater. Technol. 2021, 6, 2100591.

(39) Li, C.; Li, Z.; Nguyen, T. D. D.; Ingebrandt, S.; Vu, X. T. Real-time and multiplexed detection of sodium and potassium ions using PEDOT:PSS OECT microarrays integrated with ion-selective membranes. Electrochimica Acta 2024, 507, 145111.